Yeast-derived biosynthesis of silver/silver chloride nanoparticles and their antiproliferative activity against bacteria

Mateus Eugenio[1,7], Nathalia Müller[1], Susana Frasés[1,2,3], Rodrigo Almeida-Paes[6], Luís Maurício T. R. Lima[4], Leandro Lemgruber[1,*], Marcos Farina[5], Wanderley de Souza[1,2,3,7], Celso Sant'Anna[1,2,7,#]

[1]Laboratory of Biotechnology, Directory of Metrology Applied to Life Science, National Institute of Metrology, Quality and Technology, Duque de Caxias, RJ, Brazil; [2]National Institute of Science and Technology for Structural Biology and Bioimaging, Rio de Janeiro, RJ, Brazil; [3]Laboratory of Cellular Ultrastructure Hertha Meyer, Federal University of Rio de Janeiro, Rio de Janeiro, RJ, Brazil; [4]Laboratory of Pharmaceutical Biotechnology, Federal University of Rio de Janeiro, Rio de Janeiro, RJ, Brazil; [5]Laboratory of Biomineralization, Federal University of Rio de Janeiro, Rio de Janeiro, RJ, Brazil; [6]Micology Laboratory, Oswaldo Cruz Foundation, Rio de Janeiro, RJ, Brazil; [7]Post-graduation Program on Translational Biomedicine.

* Present Address: Welcome Trust Centre for Molecular Parasitology, University of Glasgow

[#]**Corresponding author:** cbfilho@inmetro.gov.br

Instituto Nacional de Metrologia, Qualidade e Tecnologia - Inmetro

Av. Nossa Senhora das Graças, 50, prédio 27- Xerém, 25250-020, Duque de Caxias, RJ, Brazil.

Tel: +55 2121453150 / Fax: +55 2126799837

Abstract

Here, we provided the first evidences of yeast strains assisted Ag/AgCl-NPs production *in vitro*. The formed nanoparticles were characterized by spectroscopic and electron microscopy approaches. UV-Vis supported the biosynthesis. TEM analysis evidenced that nanoparticles mainly presented circular shape and their diameter varied mostly in the range from 2 to 10 nm. XRD analysis showed a crystalline structure, with diffraction peaks corresponding to metallic silver and silver chloride nanoparticles, and when analyzed by high-resolution transmission electron microscopy (HRTEM), instead of being round, (111) (octahedral) and (200) (cubic-) symmetry facets appeared systematically in one side of the nanoparticles. Analysis of ultra-thin sections by TEM indicated that the domain of the synthesis of Ag/AgCl-NPs were mainly between cell wall and the plasma membrane. By using 3D reconstruction obtained from focused ion beam scanning electron microscopy (FIB/SEM) the spatial distribution of the domains of nanoparticles synthesis was mapped and nanoaggregates of Ag/AgCl-NPs up 35 nm in diameter were observed. Extracellular synthesis also occurred; in accordance with the fact that conditioned media from yeast isolates were as efficient at producing Ag/AgCl-NPs as live-cell cultures. Exposure of Gram-positive *Staphylococcus aureus* and Gram-negative *Klebsiella pneumoniae* cultures to Ag/AgCl-NPs led to a strong growth inhibition as shown by optical density measurements. The Ag/AgCl-NPs described here have characteristics compatible with a strong potential for use in the biotechnology industry, particularly for biomedical applications.

Keywords: Biotechnology; yeasts; metallic nanoparticles; biomimetic synthesis; silver/silver chloride nanoparticles.

1. Introduction

The field of nanotechnology has grown considerably over the past two decades, with a focus on the characterization and mass production of nanoparticles (NPs) and nanostructured materials.[1] NPs range from 1 to 100 nm in diameter and can be made from different materials, although metallic NPs have attracted particular attention in the biotechnology and material sciences, due to their intrinsic properties compared with micro-sized materials.[2] The physico-chemical properties of NPs, as well as their biomedical use, are related to their minute size, size distribution, shape, dispersion, nature and increased specific surface area.[3] NPs have a large surface area to volume ratio, which makes them particularly useful for catalytic and microbicide purposes, in industrial settings.[4-7] Currently, metallic NPs are produced by reducing noble metals such as silver,[1] gold,[8] copper,[9] zinc[10] and titanium,[11] among others.

Several kind of silver nanoparticle – including silver nanoparticles (AgNPs), silver chloride nanoparticles (AgCl-NPs) and the combination of both (Ag/AgCl-NPs) – have been synthesized by physical,[12] chemical,[13] or biological[1] processes. Currently, physical and chemical processes are the methods of choice for their synthesis. The physical methods are generally performed by sophisticated apparatus and the chemical approaches generate hazardous waste.[1] Therefore, there is an increasing demand for cheaper and ecologically friendly methods for the synthesis of silver nanoparticle types.

The green synthesis of silver nanoparticle types using biological systems represents an interesting alternative to substitute physical and chemical synthesis. Previous studies reported successful synthesis of silver nanoparticle types, especially AgNPs, assisted by biological agents, notably plant extracts,[8] and bacteria.[14] Although fungi are capable of producing silver nanoparticle types, most studies on fungal-based biosynthesis used filamentous fungi such as *Neurospora*

crassa,[15] *Trichoderma reesei,*[16] *Fusarium oxysporum,*[17] *Aspergillus niger*[18] and *Penicillium brevicompactum.*[1] Nevertheless, a few studies reported successful biosynthesis of silver nanoparticle types by single-celled fungi (i.e., yeasts), including the yeast strain MKY3,[19] *Candida albicans,*[20] *Saccharomyces boulardii*[21] and *Candida utilis.*[22] The use of yeasts for nanoparticles production is of particular interest for industry, because they represent the world's most industrially used microorganisms, and have been grown for decades in industrial-scale cultures for the production of key fermentation-based food and drink products such as bread, beer and wine.[23,24]

While the long-term knowledge of yeast cultivation for industrial applications is a strong point in favor of the use of yeasts for nanoparticles production, published data on silver-based nanoparticles production by yeasts remains limited, and there are no studies on the characterization of yeast-derived Ag/AgCl-NPs to establish their potential for industrial application. Here, 15 yeasts isolated from the digestive tract of termites were tested for their ability to produce Ag/AgCl-NPs upon incubation with silver nitrate ($AgNO_3$). We identified two isolates that were particularly efficient at producing the nanoparticles and characterized the purified Ag/AgCl-NPs by a variety of spectroscopy techniques, as well as by advanced electron microscopy. In addition, we tested the susceptibility of Gram-positive *Staphylococcus aureus* and Gram-negative *Klebsiella pneumoniae* to nanoparticle exposure.

2. Materials and Methods

2.1. Isolation of yeast strains: Yeasts were obtained from the gut of 10 termites from the species *Cornitermes cumulans.* Gastrointestinal content was plated by serial dilution onto Sabouraud agar plates, which were incubated at 28°C for 48 hours. Then, colonies were sub-

cultured in Sabouraud agar at lower densities, to allow the isolation of individual clones, which were named "TERM" (for termite).

2.2. Yeast species identification: The TERM strains most efficient at producing Ag/AgCl-NPs were subjected to species identification using the automated microbial and identification system VITEK2® (bioMérieux, Inc.), according to manufacturer's instructions.

2.3. Ag/AgCl-NPs biosynthesis and purification: Fifteen TERM isolates were screened for the biosynthesis of Ag/AgCl-NPs. Each yeast isolate was inoculated in a cell density of 10^7 cells/mL in rich liquid medium (4% glucose, 1% peptone and 1% yeast extract, pH 6.5) and was allowed to grow for 24 hours at 30°C. Then, a small volume of a 3.5 M aqueous solution of silver nitrate ($AgNO_3$) was added to the medium for a final concentration of 3.5 mM, and cultures were grown for 7 days at 30°C, in the dark, and under agitation (150 rpm). Lastly, color change was recorded photographically and the reduction of silver ions (which generates Ag/AgCl-NPs) was verified using a UV–visible Spectra Max 190 spectrophotometer, by scanning the spectrum from 200-700 nm wavelengths, with 1-nm increments. The background was cell-free culture medium without $AgNO_3$. The Cell-free control was determined by adding $AgNO_3$ to cell-free culture medium and incubating as mentioned above, and the following controls were performed: 1) yeast cultures were heated for 1 hour at 70°C before the addition of $AgNO_3$ and incubation at 30°C ('dead-cell' control); and 2) yeast cultures were centrifuged at 4,000 rpm (2720 x g) for 15 minutes, the pellet was discarded and $AgNO_3$ was added to the supernatant, before incubation at 30°C ('conditioned medium' control). For purification, the supernatant of the yeast culture medium was separated from the cell pellet by centrifugation at 4,000 rpm (2720 x g), for 15 min at room temperature, and Ag/AgCl-NPs were isolated from the supernatant by centrifugation at

15,000 rpm (38360 x g) for 20 minutes, at room temperature. The pellet containing Ag/AgCl-NPs was resuspended in a stabilizing solution of 1% sodium citrate (pH 8.0).

2.4. Scanning electron microscopy and energy-dispersive X-ray spectroscopy (SEM-EDS): Samples of yeasts cultivated in the presence of $AgNO_3$ were washed twice in PBS and allowed to adhere onto 0.1% poly-L-lysine-coated glass coverslips for 20 min, at room temperature. Then, yeasts were fixed with 2.5% glutaraldehyde and 4% paraformaldehyde in 0.1M sodium cacodylate buffer (pH 7.2, here after referred to as 'cacodylate buffer') (for 1 h at room temperature), washed in the same buffer, and post-fixed with 1% osmium tetroxide and 2.5% potassium ferrocyanide in cacodylate buffer for 45 minutes, in the dark. After washes in cacodylate buffer, samples were dehydrated in a series of ethanol solutions (30, 50, 70, 90 and 100%, for 30 min in each concentration), critical point-dried in a Leica EM CPD 030 apparatus (Wetzlar, Germany), and mounted on stubs. Dried samples were sputter coated with a 2-3-nm-thick carbon layer, using a Leica EM SCD 500 sputtering device (Wetzlar, Germany), and backscattered electron images were obtained in a Quanta FEG 450 scanning electron microscope (FEI, Netherlands), at an accelerating voltage of 5.0 kV.

For EDS analysis, purified Ag/AgCl-NPs from conditioned medium were dried at 65°C for 40 min, allowed to adhere onto carbon conductive tapes previously attached to SEM stubs and observed in a Quanta FEG 450 scanning electron microscope (FEI Company, Netherlands), equipped with an EDS unit, and operating at 20 kV. The EDAX EDS system and Genesis software were was used to identify the elements present in the sample.

2.5. X-Ray Diffraction (XRD): Powders of purified Ag/AgCl-NPs were dried at 65°C for 40 min, mounted on 10 μm thickness nylon loop supports (Hampton Research, USA) and

analyzed in a SuperNova diffractometer (Agilent), operating at 40 W (50 kV and 0.5 mA), with a CuKα radiation (1.5416 Å) in the angular range of 20°-80° (2θ angles). Measurements were properly corrected for a dark noise subtraction conducted under similar conditions. The baseline was corrected using the FityK program (http://fityk.nieto.pl/), and the XDR spectra were further analyzed by deconvolution based on a Gaussian distribution for each energy peak.

2.6. Transmission Electron Microscopy (TEM): For obtaining the diameter and shape factor of Ag/AgCl-NPs by TEM, small aliquots (5 µL) of purified nanoparticles were deposited onto Formvar-covered/carbon-coated copper grids and air-dried. Images were acquired in a Tecnai G^2 Spirit BioTWIN (FEI, Netherlands) operating at 120 kV. The diameter and shape factor of Ag/AgCl-NPs were estimated from TEM images (n = 1,200 particles/yeast strain), using the ImageJ software.[25]

2.7. High-resolution transmission electron microscopy (HRTEM): Small aliquots (5 µL) of Ag/AgCl-NPs were allowed to air dry onto a holey carbon-coated TEM grid (Electron Microscopy Sciences, USA), and imaged in a FEI Titan 80-300 transmission electron microscope (FEI, Netherlands) operating at 300 kV. High resolution images of individual Ag/AgCl-NPs were obtained and the facets of the crystallites were indexed based on the measurements of distances and angles between lattice planes. The software "*Krystal Shaper*" (© JCrystal Soft) was used for the design of the 3D model.

2.8. Ultrathin section electron microscopy: Yeasts were washed twice in PBS, fixed with 2.5% glutaraldehyde and 4% paraformaldehyde in 0.1 M sodium cacodylate buffer (pH 7.2) for 1 hour at room temperature, and post-fixed with 1% osmium tetroxide and 2.5% potassium

ferrocyanide, pH 7.3, in 0.1 M sodium cacodylate buffer, for 45 minutes in the dark. Then, samples were dehydrated in a series of acetone solutions (30, 50, 70, 90 and 100%) and embedded in Epon resin. Ultrathin sections were obtained in a Leica EM UC6 ultramicrotome, were stained with uranyl acetate and lead citrate and observed in a Tecnai G^2 Spirit BioTWIN (FEI, Netherlands), operating at 120 kV.

2.9. Focused ion beam/scanning electron microscopy (FIB/SEM): Yeast samples were resin embedded as to ultrathin sections electron microscopy described above. For FIB/SEM, trimmed tops of resin blocks were mounted in SEM stubs. An area of interest was selected and coated with a 200-nm platinum layer, and then 'slice-and-view' image series (with a step size of ~20 nm) were recorded using a FEI Helios Dual Beam microscope (FEI, Netherlands), equipped with a gallium ion source for focused ion beam 'milling'. Image series were aligned with the MIDAS program, and segmentation and 3D modeling were performed using the 3dmod program, both from the IMOD software package.[26] Videos of 3D reconstruction models were generated using QuickTime Player 7.

2.10. Antibacterial assay: The antibacterial activity of Ag/AgCl-NPs was tested against the Gram-negative *Klebsiella pneumoniae* ATCC 700603 and Gram-positive *Staphylococcus aureus* ATCC 25923 bacteria, kindly provided by Dr. Antônio Carlos Sant'Ana from Federal University of Juiz de Fora – UFJF, Minas Gerais, Brazil. The test bacteria were grown in 200 µL of either Nutrient Broth medium (Himedia) as a control condition or Nutrient Broth medium containing 10, 50, 100, 150 and 300 µg/mL Ag/AgCl-NPs in 96 well plates (Biofil®) for 24 hours at 37°C, with an initial cell density of 10^7 CFU/mL. Subsequently, the cell densities were determined by measurement of optical density at 600 nm (OD_{600}) using a UV-Visible

spectrophotometer Molecular Devices Spectra Max 190 (Sunnyvale, USA). The values obtained in the UV-Vis measurements were converted into CFU/mL as follows: *S. aureus* - OD_{600} of 1 = 1.5 x 10^9 CFU/mL[27] and *K. pneumoniae* - OD_{600} of 1 = 2.8 x 10^8 CFU/mL.[28] All analysis was carried in triplicate.

2.11. Statistical analysis: The data of the antibacterial testing were expressed as mean ± standard deviation from three independent experiments. The data were analyzed using One-Way ANOVA followed by Tukey test. $P \leq 0.05$ values were considered statistically significant.

3. Results

3.1. *Candida lusitaniae* isolates are capable of efficient Ag/AgCl-NPs production *in vitro.*

To identify yeast strains capable of efficient Ag/AgCl-NPs bioproduction, a total of 15 clonal yeast isolates from termite gut (named 'TERM' isolates) were grown in culture medium containing the nanoparticle precursor $AgNO_3$. After 7 days of growth in $AgNO_3$-containing medium, a color change (from pale yellow to brown), indicative of silver ion reduction and nanoparticle formation,[29] was observed in the culture medium of 7 TERM isolates, namely TERM73, TERM77, TERM78, TERM79, TERM82, and TERM83 (Table 1, Fig. 1A, C and Fig S1). Interestingly, a color change from pale yellow to dark brown similar to that observed for live cultures was also observed when conditioned medium from the TERM strains was incubated with $AgNO_3$, suggesting that Ag/AgCl-NPs formation also occurred extracellularly (Fig. 1A, C). In contrast, only a slight color change (from pale yellow to pale brown) was observed after

incubation of fresh culture medium containing either heat-killed yeasts or no yeast cells (i.e., 'cell-free' medium) with $AgNO_3$ (Fig. 1A, C).

Ag/AgCl-NPs formation by yeast isolates grown in the presence of $AgNO_3$ was confirmed by UV-Vis spectroscopy analysis, which showed the typical 350-450 nm absorption peak (Table 1, Fig. 1B, D and Fig. S1) attributed to the excitation of surface plasmon vibrations in silver nanoparticles.[29]

Among the 7 yeast isolates capable of Ag/AgCl-NPs production (based on medium color change and UV-Vis analysis), the most intense medium color change (to dark brown) was observed for TERM73 and TERM77, and these isolates also produced the highest UV-Vis peaks, with maximum absorbances at 415 nm and at 410 nm (Table 1 and Fig. 1). These data suggested that Ag/AgCl-NPs biosynthesis by TERM73 and TERM77 was more efficient when compared with that of the other TERM isolates; thus, these isolates were chosen for further analysis. Species identification using the Vitek® system revealed that TERM73 and TERM77 corresponded to different strains of *Candida lusitaniae*, which will be referred to, henceforth, as 'silver nanoparticle producer' (SNPP) strains 1 (SNPP1; former TERM73) and 2 (SNPP2; former TERM77).

In agreement with the color change data, conditioned media from SNPP1 and SNPP2 cultures incubated with $AgNO_3$ had similar UV-Vis profiles to those of live cultures (Fig. 1B, D) with absorption peaks at 435 nm and at 434 nm, for SNPP1 and SNPP2 conditioned media, respectively. However, the UV-Vis peaks of conditioned media were broader than those of live cultures (Fig. 1B, D), indicating that Ag/AgCl-NPs formed in $AgNO_3$-containing conditioned media have increased particle size heterogeneity. Heat-killed yeast suspensions incubated with $AgNO_3$ had maximum UV-Vis absorbance values at 349 nm and at 355 nm, for SNPP1 and SNPP2, respectively. These values were higher than those obtained for cell-free culture medium

incubated for 7 days with $AgNO_3$, suggesting that yeast extract components of the culture medium induce a basal level of Ag^+ reduction into Ag/AgCl-NPs.

3.2. SEM-EDS analysis confirms that SNPP1 and SNPP2 reduce $AgNO_3$ into particles that contain silver and chlorine atoms

SEM backscattered electron (BSE) images of SNPP1 and SNPP2 cultures incubated in the presence of $AgNO_3$ showed the topography of yeast surface decorated with several white dots of intense backscattered electron density. The atomic number contrast information provided by BSE images is indicative of Ag/AgCl-NPs formation (Fig. 2A, B). In addition, the white dots were found in the vicinity of the cells deposited onto the substrate, probably due to the presence of the recently formed nanoparticles in the extracellular medium.

We used EDS to confirm the presence of silver and chlorine atoms in the dried powder produced by cell-free conditioned media incubated with $AgNO_3$ (Fig. 2E, F). Secondary electron Images of the powdered pellet of conditioned media of SNPP1 and SNPP2 are shown in Fig. 2C, D, respectively. The EDS spectra of these samples contained a marked peak of around 3 keV (Fig. 2E, F), which is characteristic of silver atoms,[30] and peak of 2.6 KeV ascribed to chlorine.[30] EDS data strongly indicated that SNPP1 and SNPP2 synthesize Ag/AgCl-NPs *in vitro*. We also observed peaks corresponding to carbon, sulfur, potassium, sodium and oxygen in the EDS spectra of $AgNO_3$-incubated conditioned medium powder (Fig. 2E, F).

3.3. X-ray diffraction (XRD) data revealed that the Ag/AgCl-NPs produced by SNPP1 and SNPP2 have a crystalline nature.

To examine the structure of the Ag/AgCl-NPs synthesized by SNPP1 and SNPP2, we analyzed purified Ag/AgCl-NPs produced by live cells by XRD (Fig. 3). For both yeast isolates, powdered fractions of culture supernatants or conditioned media (henceforth referred as 'Ag/AgCl-NPs') yielded XRD spectra with 4 peaks at 2θ value of 38°, 45°, 64° e 78°, that were assigned to (111), (200), (220) and (311) planes of cubic crystalline phase of metallic silver (Fig. 4), which co-exist with others 7 peaks at 2θ value of 27°, 32°, 55°, 57°, 74°, 76° e 85° indexed as (111), (200), (311), (222), (400), (331) and (422) planes of cubic crystalline phase of silver chloride. This pattern obtained from the diffractogram shows that the Ag/AgCl-NPs synthesized by live yeast cells or conditioned media are crystalline, according the crystallographic analysis reported by Durán et al.[31] Our interpretation of the Ag/AgCl-NPs diffraction profiles is consistent with the standards set by the Joint Committee on Powder Diffraction standards (JCPDX, file no - 02-1098, to metallic silver, and JCPDS: 31-1238, to silver chloride nanoparticles).

3.4. Ag/AgCl-NPs are mostly spherical, and SNPP2 produces predominantly smaller Ag/AgCl-NPs, compared with those made by SNPP1 when analyzed by TEM.

We determined the size and shape factor (circularity) of the individual nanoparticles isolated from the conditioned medium by TEM (Fig. 4). Measurements of nanoparticle diameters (1,200 Ag/AgCl-NPs per yeast strain) showed that the mean diameter was 13.4 ± 14.5 nm to SNPP1 and 6.9 ± 4.5 nm to SNPP2. In addition, nanoparticles produced by SNPP1 (Fig. 4A) and SNPP2 (Fig. 4C) displayed polydispersity, with clear differences in particle sizes distributions between samples from the two strains. SNPP1 produced nanoparticles with larger distribution, from 3 to 83 nm, and SNPP2 presented narrower distribution, from 2 to 22 nm. SNPP1 cells mainly synthetized nanoparticles with 3–10 nm in diameter (59%), with a smaller proportion of

particles (32%) with diameters in the range of 11–33 nm, and fewer still (13%) with 34-83 nm in diameter (Fig. 4B). In contrast, 74% of Ag/AgCl-NPs produced by SNPP2 had 2–6 nm in diameter, with 22% of particles with diameters of 7–22 nm, and no particles with more than 22 nm in diameter were found (Fig. 4D).

The analysis of the morphology of the individual yeast produced nanoparticles based on TEM images indicated that Ag/AgCl-NPs synthetized by both yeast strains were predominantly in a spherical shape (Fig. 4A, C). These results were confirmed by circularity analysis, where a circularity value of 1 represents the perfect symmetry of a circle, while values equal or below 0.9 represents non-spherical morphologies. The evaluation of the circularity Ag/AgCl-NPs as a function of the analyzed area showed that 50-60% of nanoparticles produced by SNPP1 (Fig. 4E) and SNPP2 (Fig. 4F) appeared spherical in shape, and there were slight differences in the proportion of non-spherical morphologies between samples from the two yeast strain. According to the smaller mean diameter and size distribution, as well as the greater nanoparticle shape homogeneity data by TEM, we could infer that SNPP2 produced Ag/AgCl-NPs more suitable for biomedical applications.[3,4] In this sense, the crystalline structure and morphology of these nanoparticles were analyzed by HRTEM and their formation domain in the cell body was evaluated by ultrathin section TEM and FIB/SEM.

3.5. Ag/AgCl-NPs have octahedral and cubic hexahedral symmetry by HRTEM analysis.

The individual nanoparticle produced by SNPP2 analyzed by HRTEM displayed a well-defined crystalline structure, with interplanar distances compatible with metallic silver (Fig. 5A, B). The dashed white lines in Fig. 5A, B represent flat end faces of the nanocrystal of the type (111) (octahedral faces) and (200) (hexahedral faces). Images from the nanocrystals and the

corresponding Fast Fourier Transform (FFT) showed that the biosynthesized AgNPs have one region with flat facets (left and top regions in Fig. 5A, B, respectively) and the opposite region with a round contour (arrowheads). A model containing both (111) and (200) symmetry faces was built to show that the morphology of the crystallites correspond in part to a truncated octahedral (compare Fig. 5C with Fig. 5B).

3.6. Ultrathin section TEM shows synthesis of Ag/AgCl-NPs in cell domains between the cell membrane and the cell wall after exposure of $AgNO_3$.

In order to investigate the domain of formation of the synthetized Ag/AgCl-NPs on the yeast cell body after exposure to $AgNO_3$, we examined several SPPN2 yeasts by ultrathin section TEM. Fig. 6A depicts an ultrathin section of a representative yeast in which all Ag/AgCl-NPs were just beneath of yeast cell wall. By analyzing $AgNO_3$ treated yeasts in higher magnification images was clearly evident that the synthetized nanoparticles of different sizes – forming nanoparticle aggregates – were confined between the outer region of plasma membrane (Fig. 6B, arrowheads) and the inner region of cell wall (Fig. 6B). In some cases, Ag/AgCl-NPs dispersed inside the yeast cell wall were found (Fig. 6C), and no clear association with intracellular structures was evidenced.

3.7. FIB/SEM analysis evidenced the 3D distribution of the domain of synthesis of Ag/AgCl-NPs nanoaggregates.

The spatial distribution of Ag/AgCl-NPs using 3D reconstruction by FIB/SEM was carried out in SNPP2 cells in order to accurately map their cellular domain of formation. In the view of

the resolution of FIB/SEM used in this work, the individual Ag/AgCl-NPs were arranged into clusters in their various domain of formation (see Fig. 6B) originating structures resembling nanoscale aggregates, therefore they were hereafter referred to as "nanoaggregates". Individual serial Z-slices of yeast cells showed nanoaggregates with different sizes mostly associated with the inner region of the cell surface (Fig. 7A-E). In addition, we observed nanoaggregates in the outer surface of the cell wall and rarely the nanoaggregates were observed in the cytoplasm region (Fig. 7D, E, asterisks). Interestingly, some yeast cells exhibited very few nanoaggregates (with cytoplasmic location or associated with cell surface), while others had considerably large numbers of nanoaggregates, with a mean value of 55 nanoaggregates/cell (range: 14 - 143) (Table 2). The diameter of the nanoaggregates measured in FIB/SEM images had a broad range of size, ranging from 35 to 334 nm (mean diameter: 94 nm) (Table 2 and Fig. S2). A 3D reconstruction model spanning the thickness of an entire yeast cell gives an overall view of the entire spatial distribution of the cellular domain of formation of Ag/AgCl-NPs (Fig. 7F - I and Fig. S3). Nanoaggregates attached to the outer surface of yeast cells – likely from the synthesis of nanoparticles in the extracellular medium – were also seen.

3.8. Ag/AgCl-NPs have strong inhibitory effect on *S. aureus* and *K. pneumoniae* growth.

Ag/AgCl-NPs biosynthesized by SNPP2 were analyzed for their antiproliferative activity against *S. aureus* (Fig. 8A) and *K. pneumoniae* (Fig. 8B). Ag/AgCl-NPs after 24 hours of incubation showed remarkable antiproliferative activity against both bacterial species as shown by OD_{600}. A significant growth inhibition of both test bacteria (*K. pneumonia,* 26%, and *S. aureus,* 34%) was observed from the lowest nanoparticle concentration (10 μg/mL) when compared with the control condition. In both cases, a stronger inhibitory effect of nanoparticles exposure was

from 50 μg/mL (*K. pneumonia,* 83%, and *S. aureus,* 85%). From this concentration, the inhibition was in range 85-98% against *K. pneumoniae* and 87-98% against *S. aureus.* There was no statistically significant growth inhibition in Ag/AgCl-NPs concentration in the range of 50-300 μg/mL between the treated groups.

4. Discussion

Silver nanoparticle types, such as metallic silver nanoparticles (AgNPs), silver chloride (AgCl-NPs) and a combination of both (Ag/AgCl NPs) are currently used in an increasing number of consumer and medical products. With growing environmental and economic concerns over the use of physical/chemical processes of nanoparticle synthesis, greensynthesis of Ag/AgCl-NPs has attracted increasing attention and research efforts, with the ultimate aim of replacing harmful and expensive chemical and physical methods.[1] Despite the wealth of knowledge on industrial-scale production of consumer goods by yeasts, relatively few reports have examined the ability of yeast cells to biosynthesize metallic nanoparticles, including silver nanoparticle types.[32] To our knowledge, there is no evidence of the bioproduction of Ag/AgCl-NPs using yeast strains.

This study investigated the yeast-based production of Ag/AgCl-NPs, using a panel of 15 yeast isolates from termite gut. These termite-borne yeast strains were originally isolated due to their cellulolytic potential (SF, unpublished data); however, initial experiments showed that they were capable of considerable Ag/AgCl-NPs production. Among all isolates tested, seven were capable of Ag/AgCl-NPs production, and two isolates identified as *C. lusitaniae* strains, and named SNPP1 and SNPP2 in this work - were particularly efficient at producing Ag/AgCl-NPs (Fig. 1, Table 1, and Fig. S1). The EDS spectra of Ag/AgCl-NPs from SNPP1 and SNPP2 cultures and conditioned media showed characteristic peaks of the element silver and chlorine (Fig. 2).

Also, a combination of XRD (Fig. 3) and HRTEM-FFT (Fig. 5) analyses of purified Ag/AgCl-NPs revealed that these particles expressed octahedral (111) and cubic (200) symmetry planes although in some regions the crystallites presented a round contour. These combined data provide strong evidence that the *C. lusitaniae* isolates described here biosynthesize crystalline Ag/AgCl-NPs *in vitro*. To our knowledge, the work presented here is the first report of the bioproduction of any type of metallic nanoparticle by this *Candida lusitaniae* species.

For both yeast strains, the intensity of medium color change after incubation with the Ag/AgCl-NPs precursor $AgNO_3$ was similar, and UV-Vis analysis yielded 350-450-nm AgNPs 'signature' peaks[33] of similar shape and size (Fig 1B, D). These results suggest that SNPP1 and SNPP2 are equally effective at producing Ag/AgCl-NPs. Nevertheless, important differences were observed in the UV-Vis spectra and in the sizes of Ag/AgCl-NPs produced by SNPP1 and SNPP2 (Fig. 1). Both size and shape affect the absorption band of surface plasmon colloids, in UV-Vis spectra, with sharp bands indicating a narrower (i.e., more uniform) distribution of nanoparticle sizes and shapes.[33,34] Thus, the UV-Vis spectra of live cell cultures of SNPP1 and SNPP2, and also that of conditioned media from SNPP1, indicate that the Ag/AgCl-NPs in these samples have a narrower size and shape distribution than those observed in conditioned media of SNPP2, which yielded a broader absorbance peak, indicating a more uneven distribution. Zhang and Noguez[33] reported the following relationships between UV-Vis absorbance peaks and the shape of metallic NPs: ~385, 435, 465, 515 nm for cubical NPs; ~462 nm for truncated cubes; ~430 nm cuboctahedral NPs; ~415 nm for icosahedral NPs; and ~400 nm for spherical NPs. Based on these data, the Ag/AgCl-NPs produced by SNPP1 are likely to be cubical, truncated cubical, cuboctahedral, icosahedral and spherical, while the Ag/AgCl-NPs produced by SNPP2 are expected to be mainly cubical, cuboctahedral, icosahedral and spherical. The heterogeneity in nanoparticle morphology was evidenced by TEM analysis (Fig. 4A, B) and the circularity

measurement through the TEM images showed that the nanoparticles were mainly spherical in shape (Fig. 4E, F).

The antibacterial activity of nanoparticles varies considerably depending on the particle size, with smaller particles exhibiting higher antimicrobial activity than larger ones.[35] Thus, the small Ag/AgCl-NPs biosynthesized especially by SNPP2 (Fig 4C), which are mostly between 2 and 10 nm (Fig. 4D), are expected to have strong microbicidal activity, suitable for industrial-scale purposes. In addition, these small particles are potential candidates for use in the catalytic industry, due to their high ratio of surface area per volume.[4] Interestingly, Morones and co-workers[36] showed that the cytotoxic effect is also dependent on the types of faces found in nanoparticles, and that faces (111), such as those present in the Ag/AgCl-NPs crystals described here (Fig. 3 and 5) are highly reactive due to their high density of silver atoms. Pal and co-workers[37] showed that truncated triangular AgNPs displayed the strongest biocidal action against *E. coli*, when compared with spherical AgNPs. Overall, the combination of nanoscale size and the presence of (111) faces are expected to convey strong biocidal properties to the Ag/AgCl-NPs.

EDS spectra of the powder of Ag/AgCl-NPs contained, aside from the peaks corresponding to silver and chlorine, a number of other prominent peaks derived from yeasts or from the culture medium (carbon, oxygen, sodium and potassium) (Fig. 2E, F). The Cl^- peak may represent Cl^- that reacted with Ag^+ to form silver chloride,[38] while the Ag^+ ions that did not associate with Cl^- were reduced to Ag^0, forming AgNPs, altogether giving rise to Ag/AgCl-NPs. While the peaks for potassium and sodium may have originated from the culture medium, those for carbon and oxygen are possibly derived from the biomolecules that reduced Ag^+ ions to form Ag/AgCl-NPs, and which may have remained attached to the nanoparticle after synthesis.

The XRD analysis of purified Ag/AgCl-NPs (Fig. 3) was compatible with that described by Durán et al.,[31] who reported diffraction patterns for silver nanoparticles with Bragg peaks for

the planes (111) in (2Θ = 38º), (200) in (2Θ = 45º), (220) in (2Θ = 64º) and (311) in (2Θ = 78º), which were attributed to metallic silver and peaks for the planes (111) in (2Θ = 27º), (200) in (2Θ = 32º), (311) in (2Θ = 55º), (222) in (2Θ = 57º), (400) in (2Θ = 74º), (331) in (2Θ = 76º) and (331) in (2Θ = 85º), which were ascribed to silver chloride nanoparticles.

We also observed a basal level of Ag/AgCl-NPs formation in fresh medium (i.e., with no interference of yeast biological activity) and in culture medium containing heat-killed yeasts (Fig. 1). However, the production of Ag/AgCl-NPs independent of the presence of live yeasts or of secreted yeast molecules (such as those expected to be found in the conditioned medium) was considerably reduced compared with that observed in live cell cultures or in conditioned media. It is possible that the yeast extract present in the culture medium induced some level of Ag/AgCl-NPs formation. On the other hand, the reduction of silver ions to form silver nanoparticles can be accomplished by many compounds nonbiological or biological.[13,31] Based on that, it is possible that components of the culture medium other than the yeast extract could also induce Ag/AgCl-NPs formation.

We used ultrathin section TEM to investigate the surface-associated sites of Ag^+ reduction to form Ag/AgCl-NPs in SNPP2 cells (Fig. 6). Such method was reliable to accurately show the domain the nanoparticles formation in SNPP2 exposure to $AgNO_3$. This was the first evidence of metallic nanoparticle formation in the space confined between the outer region of plasma membrane and the inner region of cell wall of yeast. The FIB/SEM 3D-reconstruction data of yeasts incubated with $AgNO_3$ provided an interesting overview of the spatial distribution of those nanoparticles synthesis cellular location (Fig. 7). The biosynthesis of Ag/AgCl-NPs in such cell region might by assisted by cell surface molecules; however, this is a complex issue that requires further in-depth studies to readily understand their mechanism of formation. In addition, nanoparticles aggregates decorating the outermost region of the cell wall were found (Fig. 2, 6 and

7). Nevertheless, further analysis is required to determine if the surface-associated Ag/AgCl-NPs observed in SEM images were transported from the intracellular environment or deposited from the culture medium onto the cell surface. We did not observe a clear association between Ag/AgCl-NPs agglomerates and intracellular organelles. In other green systems, silver types nanoparticles biosynthesis is either intracellular,[39,40] extracellular[1,19] or both[41].

Ions Ag^+ and other silver-based compounds have been used for a long time as an antimicrobial agent because they have a strong inhibitory effect against a wide range of microorganisms.[42-45] The evaluation of antimicrobial activity of silver nanomaterials biologically synthesized has grown considerably in recent years,[46,47] however there are few reports when compared to studies with nonbiological.[48] Silver nanoparticles have been tested against bacteria arranged in biofilms,[43, 49] which is more resistant to antibiotics. The rapid development of multi-resistant bacteria due to the indiscriminate use of antibiotics becomes a serious issue that deserves significant attention to the development of new alternative therapies. *S. aureus* infection causes disorders ranging from a simple infection (pimples, minor skin infection, boils and cellulitis) to severe clinical situations (pneumonia, meningitis, endocarditis, toxic shock syndrome and others), while *K. pneumoniae* infection causes severe pulmonary diseases, although it is commonly an agent of nosocomial infections (urinary tract, and wounds). Although the infection of both bacteria is significantly greater in patients with compromised immune systems, they are resistant to a large number of antibiotics, being, therefore, agents of clinical and public health problems.[47-49]

The bacteria here tested were susceptible to strong growth inhibition after exposure to Ag/AgCl-NPs from their lowest concentration tested (10 μg/mL) and concentrations between 50-300 μg/mL were very aggressive (Fig. 8). Soo-Hwan et al.[50] showed that total growth inhibition of *S. aureus* using chemically produced AgNPs was at 100 μg/mL. On the other hand, at the 50 μg/mL concentration, an insignificant decrease of bacterial growth was seen. Sen et al.[51] found

that the biosynthesized AgNPs and stabilized by β-glucan isolated from *Pleurotus florida* totally inhibit the growth of *K. pneumoniae* after treatment with 40 μg/mL.

Collectively, the bioproduced Ag/AgCl-NPs here presented is a promising alternative to antibiotics commonly used in terms of antiproliferative effect against *S. aureus* and *K. pneumoniae*. In addition, further optimization studies of particle production can be carry out to improve their antibacterial performance.

5. Conclusion

In the present study, the yeast-assisted synthesis of Ag/AgCl-NPs was showed for the first time. Importantly, we provided a strong morphological evidence of the nanoparticle cellular domain of synthesis – an issue that is poor understood. The nanoparticles were characterized by spectroscopic and electron microscopy approaches and the nature, crystallinity, shape, size, and size dispersity seem to be beneficial for their application. Our findings showed that the eco-friendly Ag/AgCl-NPs produced by yeast strains have a structure compatible with their use in industrial biotechnology, particularly in the microbicidal industries. Further studies are now required to test directly the potential of these Ag/AgCl-NPs for industrial use, and to optimize their production.

6. Acknowledgements

This work was supported by National Council for Scientific and Technological Development (CNPq), the Carlos Chagas Filho Foundation for Research Support of the State of Rio de Janeiro (FAPERJ) and Coordination for the Improvement of Higher Education Personnel (CAPES). The authors would like to thank Mr. Luis Sérgio Cordeiro for technical support.

7. References

1 K. S. H. Naveen, G. Kumar, L. Karthik and K. V. B. Rao, *Arch. Appl. Sci. Res*., 2010, **2**, 161–167.

2 W. Wu, Q. He and C. Jiang, *Nanoscale Res. Lett*., 2008, **3**, 397–415.

3 G. Schmid, *Nanoparticles: From Theory to Application*, Wiley-VCH: Weinheim, 2004.

4 C. Buzea, I. I. P. Blandino and K. Robbie, *Biointerphases*, 2007, **2**, 17–71.

5 S. K. Das, M. M. R. Khan, A. K. Guha and N. Naskar, *Green Chem.*, 2013, **15**, 2548-2557.

6 S. K. Das, T. Parandhaman, N. Pentela, A. K. M. M. Islam, A. B. Mandal and M. Mukherjee, *J. Phys. Chem. C*, 2014, **118 (42)**, 24623–24632.

7 S. K. Das, M. M. R. Khan, A. K. Guha, A. R. Das and A. B. Mandal, *Bioresour. Technol.*, 2012, **124**, 495–499.

8 J. L. Huang, Q. B. Li, D. H. Sun, Y. Lu, Y. Su, X. Yang, H. Wang, Y. Wang, W. Shao, N. He, J. Hong and C. Chen, *Nanotechnology*, 2007, **18**, 10.

9 R. A. Soomro, S. T. H. Sheraz, Sirajuddin, N. Memon, M. R. Shah, N. H. Kalwar, K. R. Hallam and A. Shah, *Adv. Mat. Lett.*, 2014, **5**, 191–198.

10 S. Nagarajan and K. A. Kuppusamy, *J. Nanobiotechnology*, 2013, **11**, 39.

11 H. Shi, R. Magaye, V. Castranova and J. Zhao, *Part. Fibre Toxicol.*, 2013, **10**, 15.

12 F. Mafuné, J. Kohno, Y. Takeda and T. Kondow, *J. Phys. Chem. B.*, 2000, **104**, 8333–8337.

13 D. L. V. Hyning and C. F. Zukoski, *Langmuir*, 1998, **14**, 7034–7046.

14 P. Jeevan, K. Ramya and A. E. Rena, *Indian J. Biotechnol.*, 2012, **11**, 72–76.

15 E. Castro-Longoria, A. Vilchis-Nestor and M. Avales-Borja, *Colloids Surf. B Biointerfaces*, 2011, **83**, 42–48.

16 K. Vahabi, G. A. Mansoori and S. Karimi, *Insciences J.*, 2011, **1**, 65–79.

17 N. Durán, P. D. Marcato, O. L. Alves, G. I. H. Souza and E. Esposito, *J. Nanobiotechnology*, 2005, **3**, 8.

18 G. Sagar and B. Ashok, *Euro. J. Exp. Bio.*, 2012, **2**, 1654–1658.

19 M. Kowshik, S. Ashtaputre, S. Kharrazi, W. Vogel, J. Urban, S. K. Kulkarni and K. M. Paknikar, *Nanotechnology*, 2003, **14**, 95–100.

20 A. H. Atef, K. M. Mogda and H. H. Mahmoud, *N. Y. Sci. J.*, 2013, **6**, 27–34.

21 A. Kaler, S. Jain and U. C. Banerjee, *Biomed Res. Int.*, 2013, **2013**, 872940.

22 S. R. Waghmare, N. M. Mulla, S. R. Marathe and K. D. Sonawane, *3 Biotech.*, 2015, **5**, 33–38.

23 C. N. Frey, *Ind. Eng. Chem.,* 1930, **22**, 1154–1162.

24 G. M. Walker, *Yeast physiology and biotechnology*, John Wiley & Sons: New Jersey, 1998.

25 C. A. Schneider, W. S. Rasband and K. W. Eliceiri, *Nat. Methods*, 2012, **9**, 671–675.

26 J. R. Kremer and D. N. Mastronarde, *J. Struct. Biol.*, 1996, **116**, 71–76.

27 J. H. Melehani, D. B. A. James, A. L. DuMont, V. J. Torres and J. A. Duncan. *PLoS Pathog.*, 2015, **11**, 6.

28 C. H. Hung, C. F. Kuo, C. H. Wang, C. M. Wu and N. Tsao. *Antimicrob. Agents Chemother.*, 2011, **55**, 1358-1365.

29 S. Elumalai and R. Devika, *Int. J. Pharm. Res. Sci.*, 2014, **02**, 98–103.

30 V. Gopinath, S. Priyadarshini, N. M. Priyadharsshini, K. Pandian and P. Velusamy, Linn. *Mater. Lett.*, 2013, **91**, 224–227.

31 N. Durán, R. Cuevas, L. Cordi, O. Rubilar and M. C. Diez, *SpringerPlus*, 2014, **3**, 645.

32 K. Quester, M. Avalos-Borja and E. Castro-Longoria, *Micron*, 2013, **54–55**, 1–27.

33 J. Z. Zhang and C. Noguez, *Plasmonics*, 2008, **3**, 127–150.

34 Z. H. Mbhele, M. G. Salemante, C. G. C. E. V. Sittert, J. M. Nedeljkovic, V. Djokovic and A. S. Luyt, *Chem. Mater.*, 2003, **15**, 5019–5024.

35 N. Durán, P. D. Marcato, R. D. Conti, O. L. Alves, F. T. M. Costa and M. Brocchi, *J. Braz. Chem. Soc.*, 2010, **21**, 949–959.

36 J. R. Morones, J. L. Elechiguerra, A. Camacho, K. Holt, J. B. Kouri, J. T. Ramírez and M. J. Yacaman, *Nanotechnology*, 2005, **16**, 2346–2353.

37 S. Pal, Y. K. Tak and J. M. Song, *Appl. Environ. Microbiol.*, 2007, **73**, 1712–1720.

38 T. W. G. Solomons, *Organic Chemistry*, John Wiley & Sons: New York, 1996.

39 H. Korbekandi, Z. Ashari, S. Iravani and S. Abbasic, *Iran J. Pharm. Res.*, 2013, **12**, 289–298.

40 S. Mirunalini, V. Arulmozhi, K. Deepalaskhmi and M. Krishnaveni, *Not. Sci. Biol.*, 2012, **4**, 55–61.

41 N. Samadi, D. Golkaran, A. Eslamifar, H. Jamalifar, M. R. Fazeli amd F. A. Mohseni, *J. Biomed. Nanotechnol.*, 2009, **5**, 247–253.

42 T. Parandhaman, A. Das, B. Ramalingam, D. Samanta, T. P. Sastry, A. B. Mandal and S. K. Das. *J. Hazard. Mater.*, 2015, **290**, 117–126.

43 P. Thuptimdanga, T. Limpiyakornb, J. McEvoye, B. M. Prüße and E. Khanf. *J. Hazard. Mater.*, 2015, **290**, 127–133.

44 S. Galdiero, A. Falanga, M. Vitiello, M. Cantisani, M. Marra and M. Galdiero. *Molecules*, 2011, **16**, 8894-8918.

45 A. M. Allahverdiyev, E. S. Abamor, M. Bagirova, C. B. Ustundag, C. Kaya, F. Kaya and M. Rafailovich. *Int. J. Nanomedicine*, 2011, **6**, 2705–2714.

46 G. Singh, P. K. Babele, S. K. Shahi, R. P. Sinha, M. B. Tyagi and A. Kumar. *J. Microbiol. Biotechnol.*, 2014, **24**, 1354–1367.

47 S. K. Fridkin. *Clin. Infect. Dis.*, 2001, **32**,108-115.

48 D. L. Paterson, W. C. Ko, A. Von Gottberg, S. Mohapatra, J. M. Casellas, H. Goossens, L. Mulazimoglu, G. Trenholme, K. P. Klugman, R. A. Bonomo, L. B. Rice, M. M. Wagener, J. G. Mccormack and V. L. Yu. *Clin. Infect. Dis.*, 2004, **39**, 31-37.

49 N. Woodford, P. M. Tierno, K. Young, L. Tyssal, M. F. Palepou, E. Ward, R. E. Painter, D. F. Suber, D. Shungu, L. L. Silver, K. Inglima, J. Kornblum and D. M. Livermore. *Antimicrob. Agents Chemother.*, 2004, **48**, 4793-4799.

50 K. Soo-Hwan, H. S. Lee, D. S. Ryu, S. J. Choi and D. S. Lee. *Korean J. Microbiol. Biotechnol.*, 2011, **39**, 77–85.

51 I. K. Sen, A. K. Mandal, S. Chakraborti, B. Deya, R. Chakraborty and S. S. Islam. 2013. *Int. J. Biol. Macromol.*, **62**, 439– 449.

8. Figure legends

Figure 1. Direct visualization and UV-visible spectroscopy analysis of silver nanoparticle (Ag/AgCl-NPs) bioproduction by *Candida lusitaniae* strains. Cultures of *C. lusitaniae* SNPP1 (former TERM73) (Fig. 1A, B) and SNPP2 (former TERM77) (Fig. 1C, D) were incubated with 3.5 mM of the Ag/AgCl-NPs precursor $AgNO_3$ (at 30°C, for 7 days, and under agitation), and then photographed (Fig. 1A, C) and analyzed by UV-visible spectroscopy (Fig. 1B, D). Background, cell-free culture medium without $AgNO_3$; Cell-free control, culture medium with 3.5 mM $AgNO_3$; Live cultures, cultures grown in the presence of $AgNO_3$; Dead-cell control, culture medium containing yeasts killed by heating (at 70°C, for 1h) and then incubated with $AgNO_3$; Conditioned medium, culture supernatants incubated with $AgNO_3$.

Figure 2. Scanning electron microscopy (SEM) and energy-dispersive X-ray spectroscopy (EDS) analysis of the product formed after addition of aqueous $AgNO_3$ to *Candida lusitaniae* yeast cultures or conditioned medium. Fig. 2A and Fig. 2B - Backscattered electron images of *C.* SNPP1 (Fig. 2A) and SNPP2 (Fig. 2B) cells after incubation with $AgNO_3$ for 7 days at 30°C, showing numerous white dots on the cell surface and on the substrate, likely corresponding to Ag/AgCl-NPs. Fig. 2C and Fig. 2D - Secondary electron images of air-dried Ag/AgCl-NPs purified from SNPP1 (Fig. 2C) and SNPP2 (Fig. 2D) conditioned media that had been incubated

with $AgNO_3$. Fig. 2E and Fig. 2F - Corresponding EDS spectra of the samples shown in Fig. 2C and Fig. 2D, respectively.

Figure 3. **X-ray diffraction (XRD) patterns.** XRD analysis of the Ag/AgCl-NPs biosynthesized by SNPP1 (Fig. 3A) SNPP2 (Fig. 3B) live cell cultures, after incubation with $AgNO_3$ for 7 days, at 30°C, showing peaks corresponding to lattice planes (111), (220), (220) and (311) ascribed as metallic silver nanoparticles, as well as lattice planes (111), (200), (311), (222), (400), (331) and (331) matched to silver chloride nanoparticles.

Figure 4. Particle diameter and shape factor (circularity) analyses by transmission electron microscopy (TEM) of the Ag/AgCl-NPs synthesized by *Candida lusitaniae* strains. Low magnification representative TEM images of Ag/AgCl-NPs produced by SNPP1 (Fig. 4A) and SNPP2 (Fig. 4C), and histograms of particle size distributions in Fig. 4B and Fig. 4D. Circularity analysis of Ag/AgCl-NPs produced by SNPP1 (Fig. 4E) and SNPP2 (Fig. 4F), where a value of 1 represents perfect circular symmetry.

Figure 5. High-resolution transmission electron microscopy (HRTEM) of the nanoparticles biosynthesized by SNPP2. Fig. 5A, B - HRTEM images of individual AgNPs, with cubic symmetry faces (200) and octahedral symmetry faces (111). The inset in B shows the Fast Fourier transform of the crystal image from where the lattice distances were obtained. Fig. 6C - Model of a crystal that presents cubic and octahedral faces symmetrically arranged, observed in the [0-11] zone axis.

Figure 6. Ultrathin section TEM of yeast exposed to $AgNO_3$. Fig. 6A - Longitudinal section showing the general morphology of yeast after exposure to $AgNO_3$ where it is possible to observe several Ag/AgCl-NPs agglomerates associated with inner part of cell surface (arrows). Fig. 6B - High magnification TEM image showing formed Ag/AgCl-NPs between plasma membrane (arrowheads) and cell wall (CW). Fig. 6C - Thin section of yeast presenting formed Ag/AgCl-NPs distributed through the cell wall (CW).

Figure 7. Focused ion beam scanning electron microscopy (FIB/SEM) analysis of SNPP2 cells containing Ag/AgCl-NPs. Fig. 7A-E - Z-slices from one representative yeast cell containing Ag/AgCl-NPs nanoaggregates (arrows) associated with the cell surface and outside the cells. Note that the nanoaggregates were mostly associated with the inner part of the cell wall (arrowheads). In few cases, nanoaggregates were found in the cell cytoplasm (Fig. 7D, E, asterisks). Fig. 7F - I) - Different views of a 3D model showing the spatial distribution of Ag/AgCl-NPs nanoaggregates inside and outside a yeast cell. Green, outermost cell wall layer; yellow, innermost cell wall layer; silver, Ag/AgCl-NPs nanoaggregates.

Figure 8 - Effect of Ag/AgCl-NPs on growth of *Staphylococcus aureus* and *Klebsiella pneumonia.* Optical density measurements at 600nm of *S. aureus* (Fig. 7A) and *K. pneumonia* (Fig. 7B) exposed to 10, 50, 100, 150 and 300 μg/mL Ag/AgCl-NPs in 96-well plate experiments. The data were expressed as mean ± standard deviation from three independent experiments. $P \leq 0.05$ values were considered statistically significant. Similar letters represent no significant difference between groups.

Electronic Supplementary Material 1 – Culture medium color change and UV-Vis spectrum of yeast isolates other them SNPP1 (former TERM73) and SNPP2 (former TERM77). Cell culture medium color change and UV-Vis analysis of yeast grown in the presence of 3.5 mM $AgNO_3$ for 7 days from TERM isolates (TERM 78, TERM 79, TERM82, TERM 83 and TERM 89) capable of producing Ag/AgCl-NPs.

Electronic Supplementary Material 2 – Diameter of intracellular Ag/AgCl-NPs nanoaggregates. Fig. 2S – Frequency of intracellular Ag/AgCl-NPs agglomerates of different sizes (diameters) based on focused ion beam/scanning electron microscopy (FIB/SEM) Z-stacks of yeast cells from *C. lusitaniae* SNPP2 cells.

Electronic Supplementary Material 3 - Movie of focused ion beam scanning electron microscopy (FIB/SEM) series of the cell shown in Fig. 8A - E. The FIB-SEM series originated a 3D model from an entire yeast, allowing the visualization of the spatial distribution of Ag/AgCl-NPs agglomerates in the inner part of the cell, as well as inside the cell wall and in the external medium. Green – outermost cell wall surface; yellow – innermost cell wall surface; silver – Ag/AgCl-NPs agglomerates.

Table 1 - Screening of yeast isolates capable of producing Ag/AgCl-NPs.

Yeast isolate	Medium color change	UV-Vis absorbance (a.u.)
TERM73 (SNPP1)	Dark Brown	2.75

TERM77 (SNPP2)	Dark Brown	3.13
TERM78	Light Brown	1.68
TERM79	Light Brown	1.90
TERM82	Light Brown	1.74
TERM83	Light Brown	1.89
TERM89	Light Brown	1.77

Medium color change and UV-Vis analysis of isolated yeast strains grown for 7 days in the presence of the silver nanoparticle (Ag/AgCl-NPs) precursor $AgNO_3$.

Table 2 - Measurement of Ag/AgCl-NPs aggregates through the FIB/SEM image series.

Intracellular Ag/AgCl-NPs nanoaggregates	Number/ diameter
Mean number (range)	55 (14 – 143)
Mean diameter, in nm (range)	94 (35 – 334)

The measurements were carried out in FIB/SEM Z-section of 20 SNPP2.

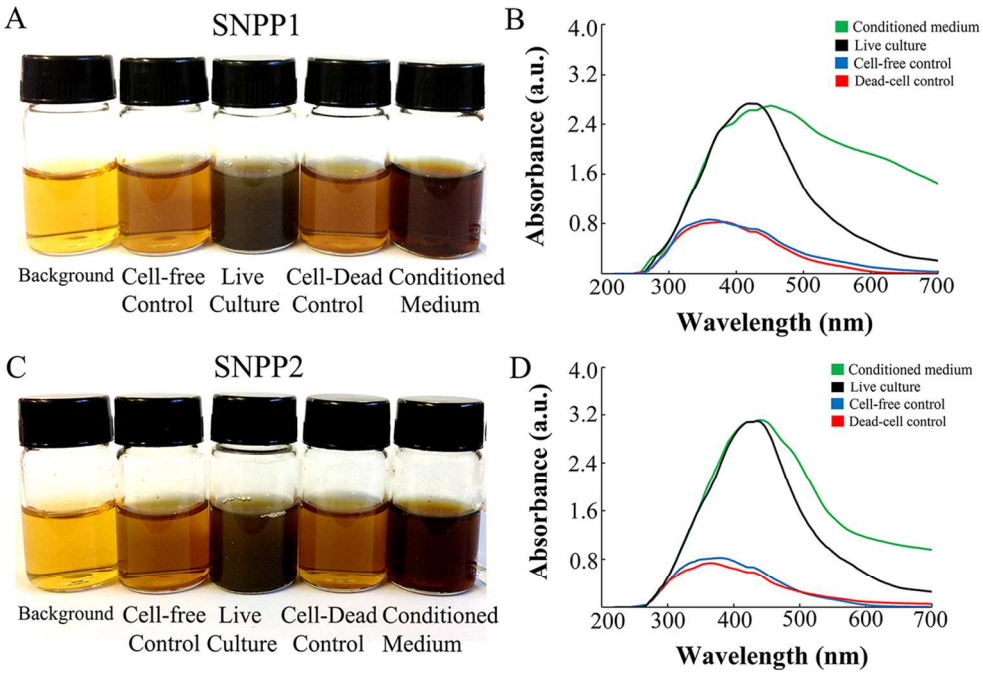

119x80mm (300 x 300 DPI)

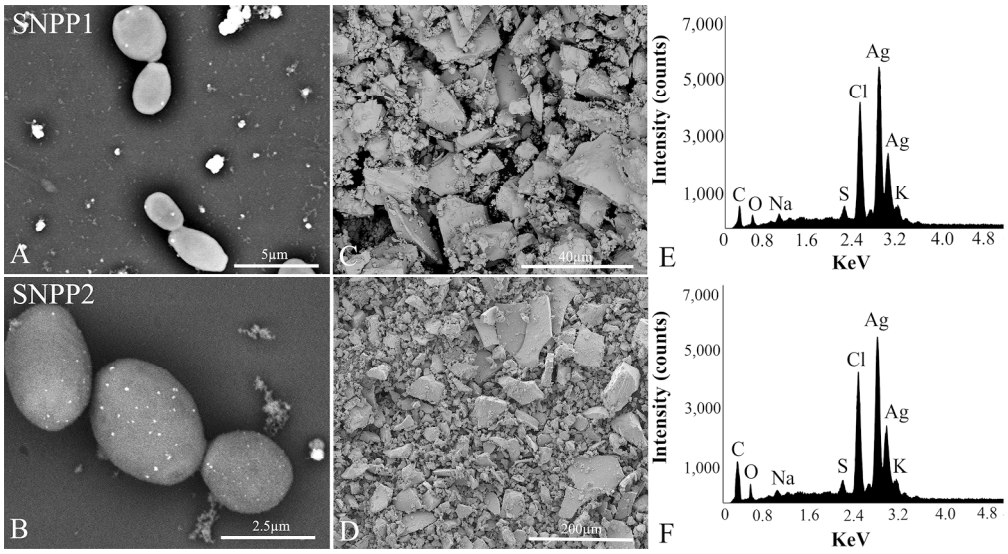

199x108mm (300 x 300 DPI)

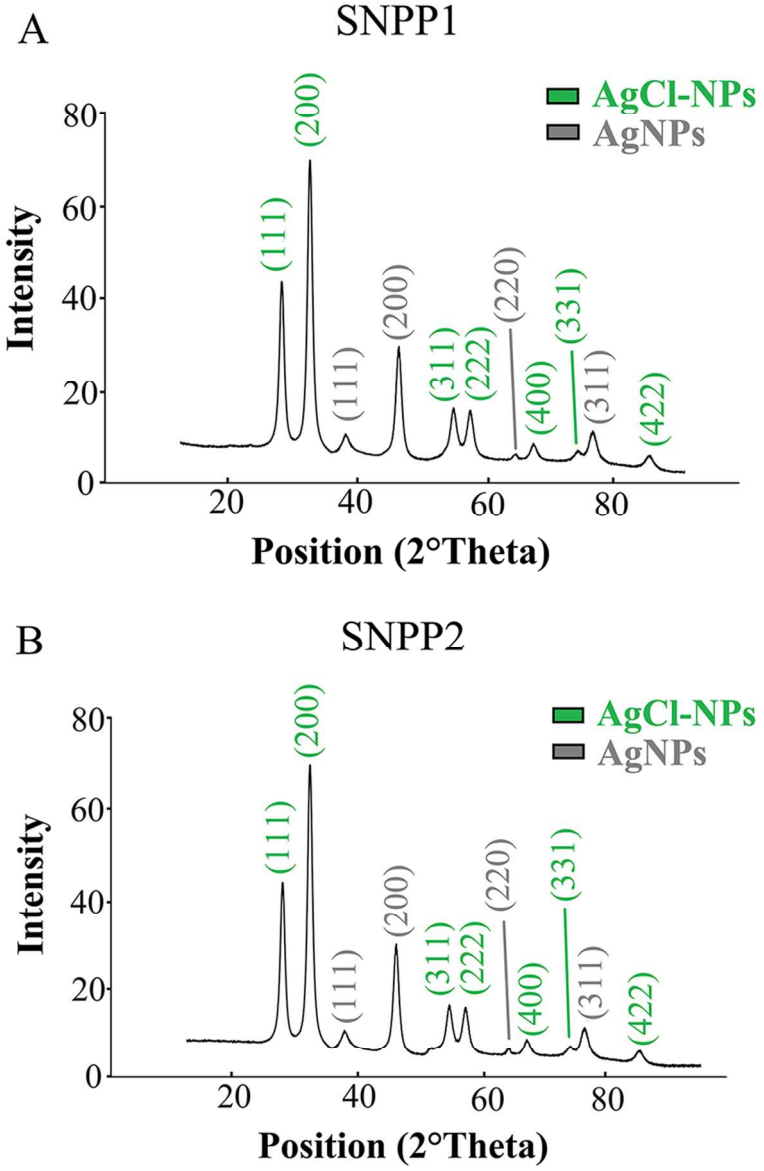

80x123mm (300 x 300 DPI)

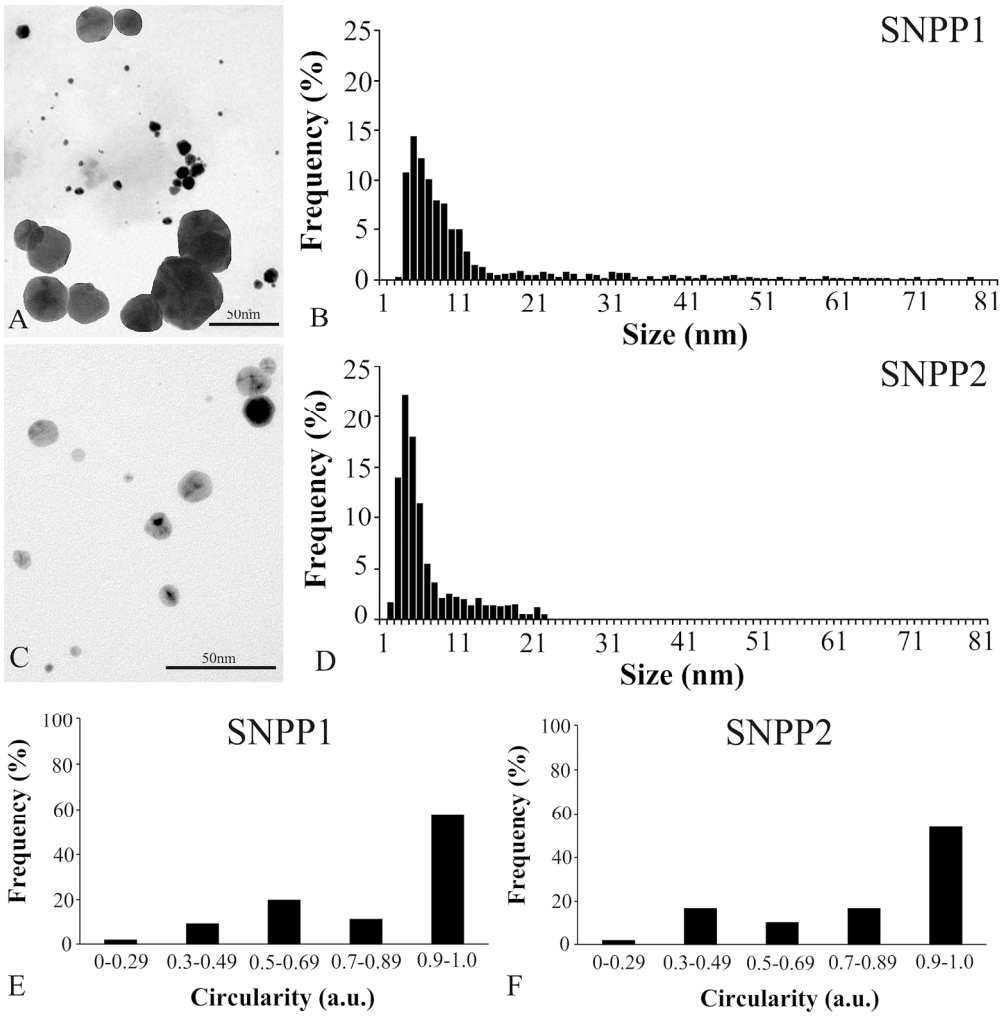

180x182mm (300 x 300 DPI)

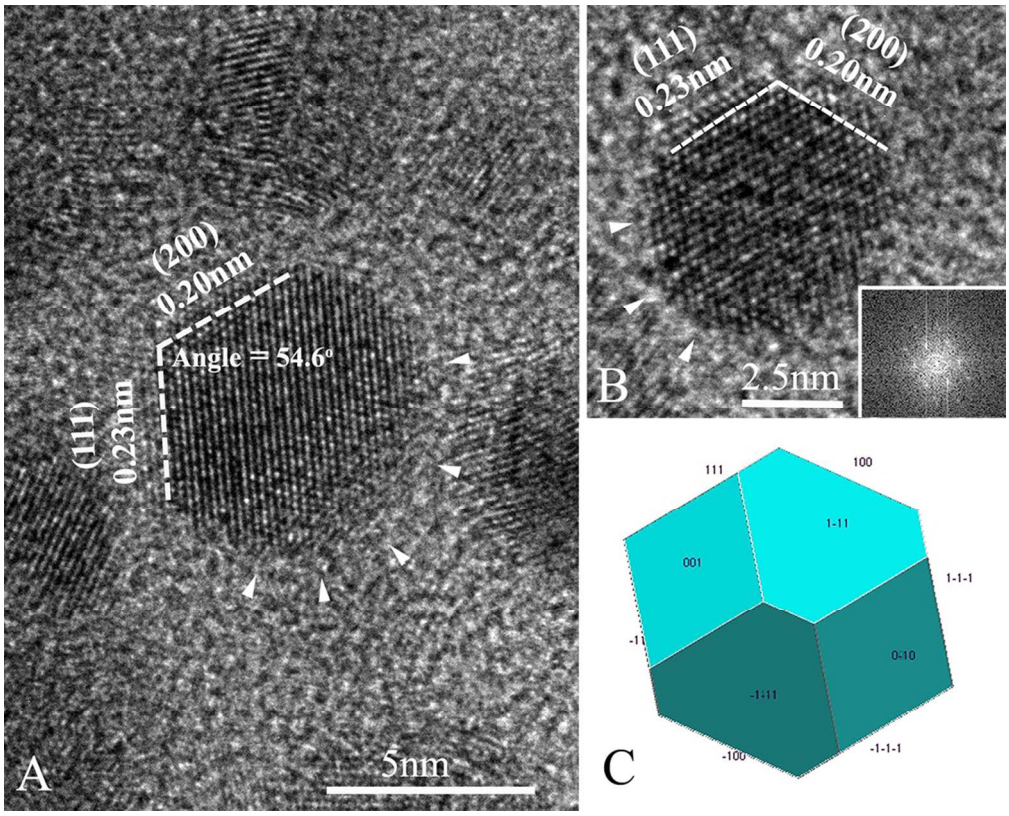

99x80mm (300 x 300 DPI)

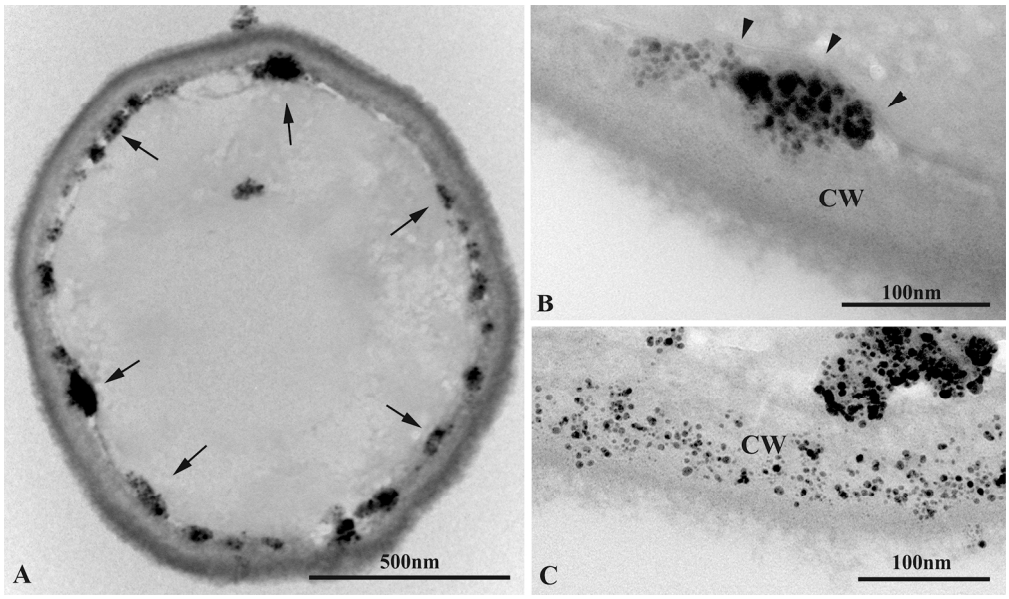

180x105mm (300 x 300 DPI)

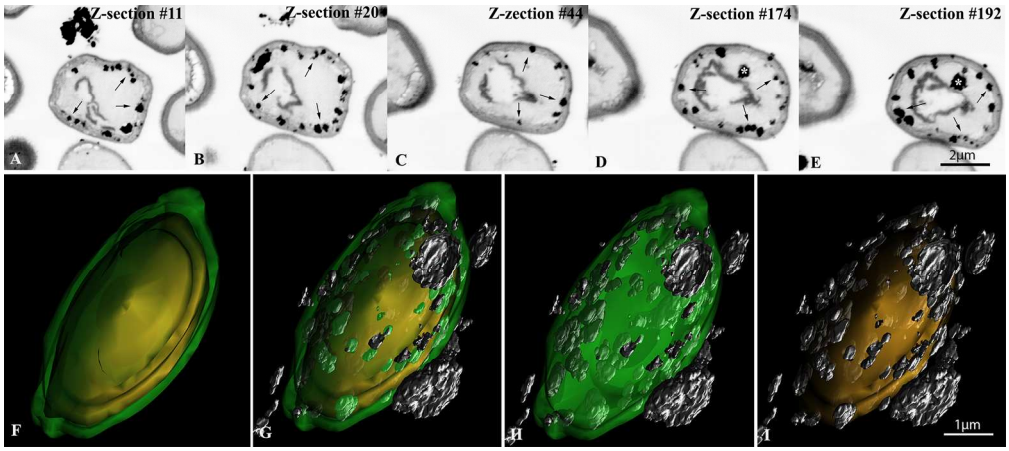

180x79mm (300 x 300 DPI)

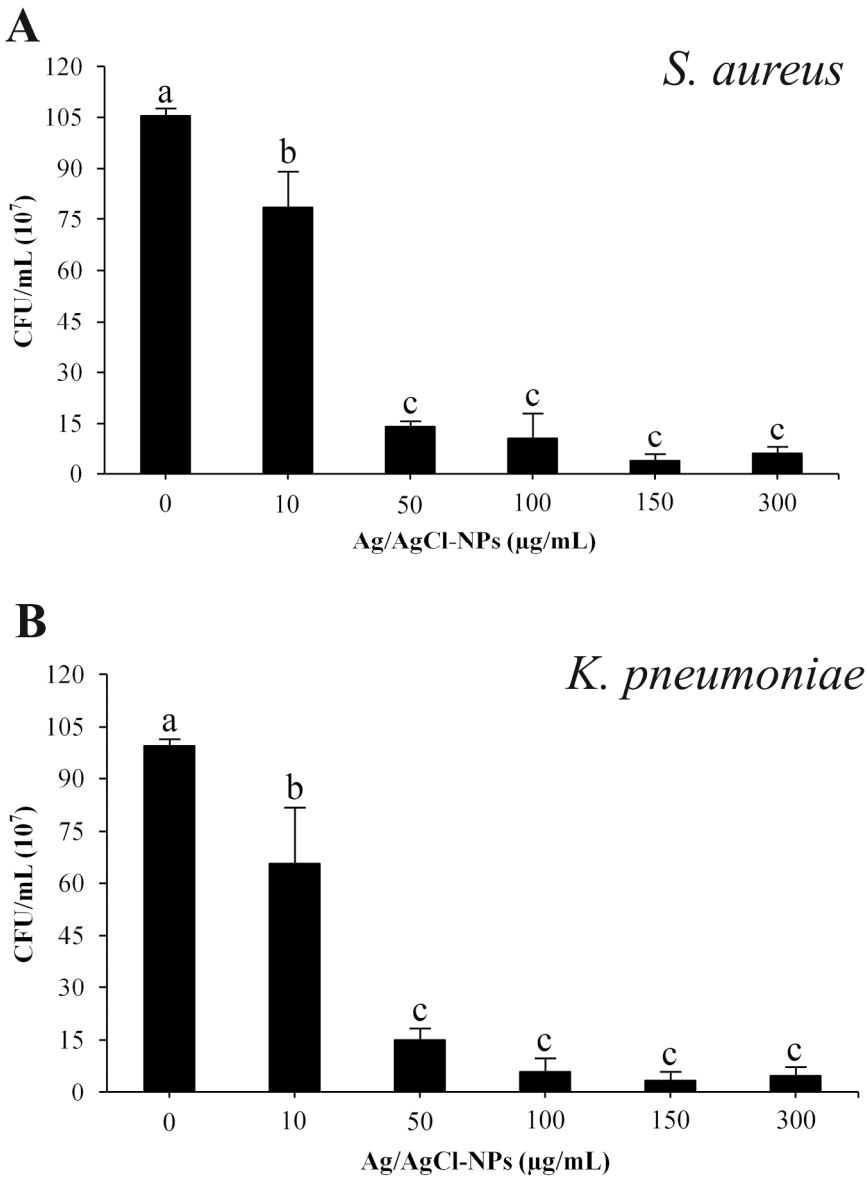

196x257mm (300 x 300 DPI)

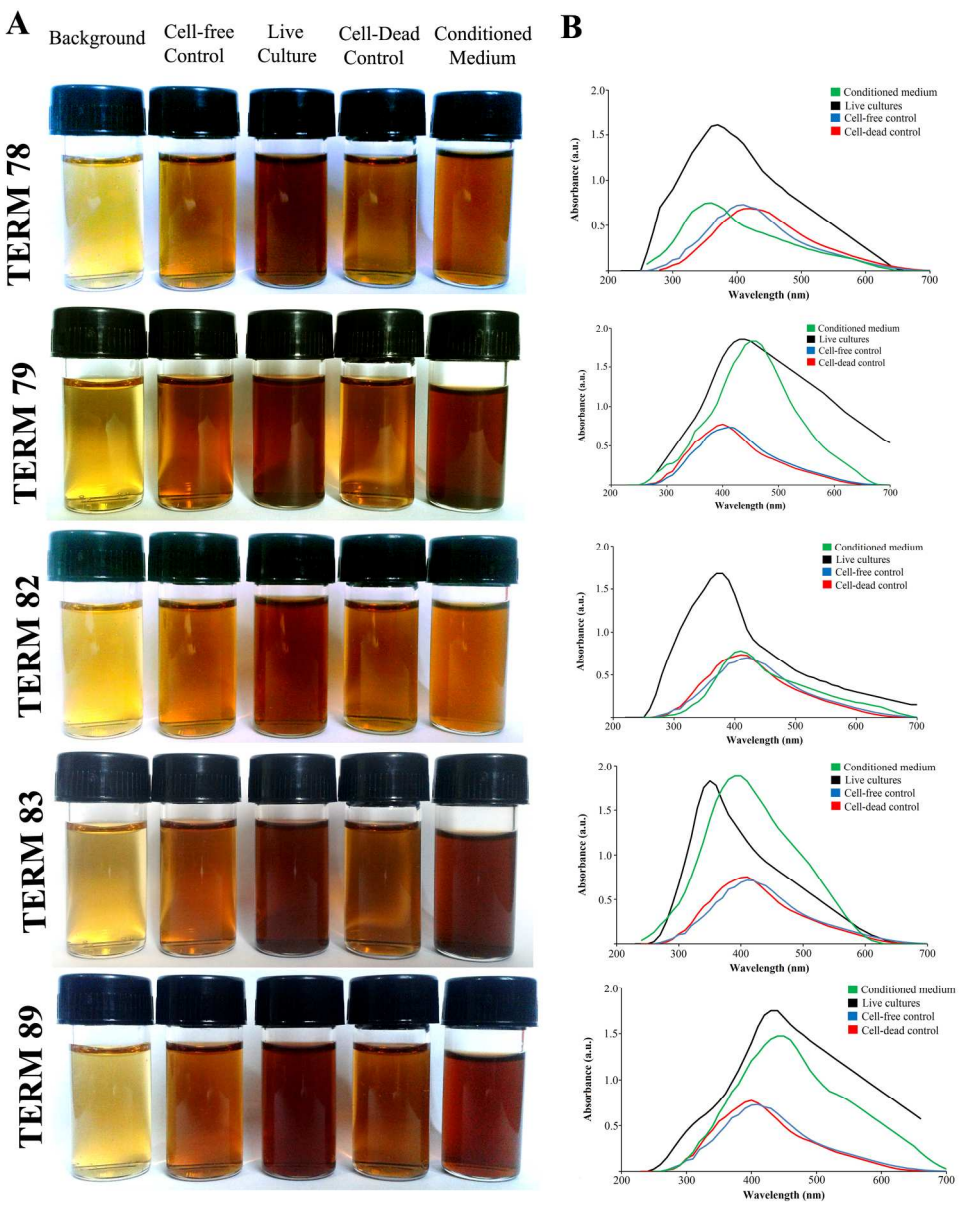

201x250mm (300 x 300 DPI)

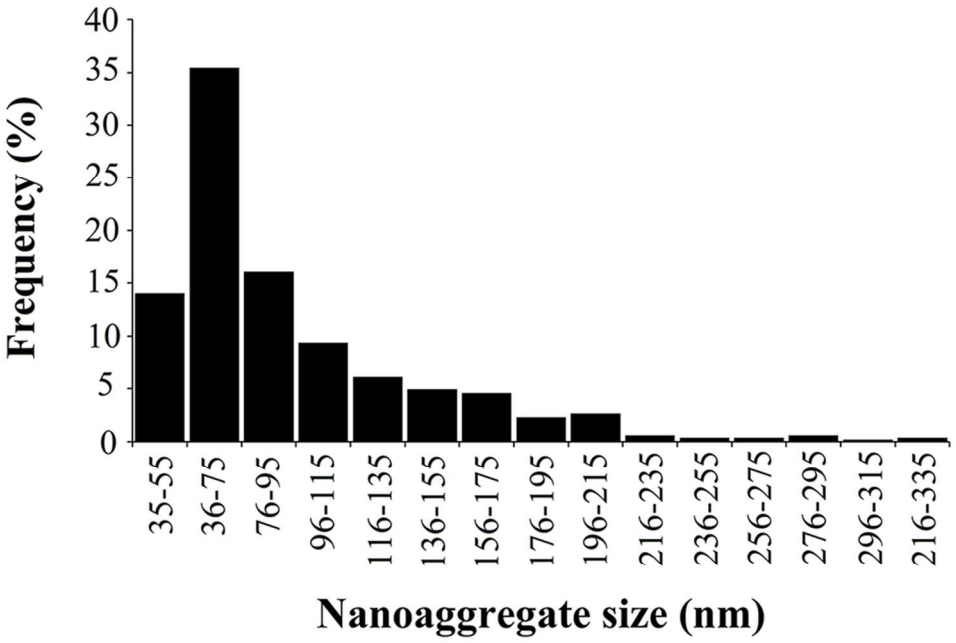

90x60mm (300 x 300 DPI)